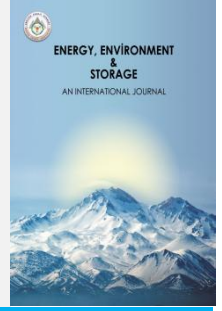




# Energy, Environment and Storage

JournalHomepage: [www.enenstrg.com](http://www.enenstrg.com)



## Investigation of the Performance Changes of the Savonius Wind Turbine Rotors with the Same Front View Area of Look by Change of the Aspect Ratio

Mahmut Burak Akkus<sup>1</sup>, Zeki Haksever<sup>2</sup> and Süleyman Osmanlı<sup>3</sup>

<sup>1</sup>Erciyes University, Faculty of Engineering, Department of Mechanical Engineering, Kayseri, Türkiye

<sup>1</sup>mbakkus54@gmail.com, ORCID:0000-0002-4561-7093,

<sup>2</sup>Erciyes University, Faculty of Engineering, Department of Mechanical Engineering, Kayseri, Türkiye

<sup>2</sup>zhaksever@gmail.com, ORCID: 0000-0001-7037-4540

<sup>3</sup>Van Yuzuncuyil University, Faculty of Engineering, Department of Mechanical Engineering, Van, Türkiye

<sup>3</sup>steksin@yyu.edu.tr, ORCID: 0000-0001-8854-0332

**ABSTRACT.** In this study, Savonius type wind turbine rotors with the same front view area were produced with 3D printers by changing their aspect ratios, and then both experimental and numerical analyzes were carried out according to them attaching end plate and without end plate situations. The wind tunnel in the university was used in the experimental analysis. For numerical analysis, rotors and wind tunnels modeled in SolidWorks CAD program were analyzed in Ansys Fluent program. The analyzes made are for imaging purposes only, and the results in the experimental analyzes are accepted as correct. The reduction of aspect ratios in the uncapped analyzes decreased the overall efficiency, but the opposite effect was observed when the analyzes were repeated with the end plate. In addition, while negative pressure was observed in the rotors made without end plate (bare case) in the digital images, this situation was not seen in the analyzes made with the end plate.

**Keywords:** Wind Turbines, Savonius, Tip Speed Ratio, Power Factor, Pressure

**Doi:** <https://doi.org/10.52924/WFVI2347>

### 1. INTRODUCTION

Humanity has needed energy to live for generations. Some attempts have been made to do this, both from the nutrients they get for survival and to make their daily life comfortable. Especially after the industrial revolution, to meet the rapidly increasing energy need, this need has been tried to be met by first using water vapor and then fossil fuels. However, as a result of this, the rapid deterioration of the world ecosystem has made it possible to switch to alternative energy production methods. The reason for this is the emergence of gases that disrupt the ecosystem and pollute the atmosphere while obtaining energy from fossil fuels. The electrical energy that we use frequently today can be obtained through various transformations, even if it is not found directly in nature. In electricity generation, natural resources are always produced by using a turbine or turbine group with subsequent generators [1-2].

Due to the increasing energy demand and climate change based energy crises recently, electricity generation from other natural sources has become increasingly common. But still, fossil fuels are widely used due to the need of improvement of renewable energy implication [3].

Although each of the researched subjects in this study are included in the literature studies separately. Akkuş et al. [4] experimentally and numerically examined the performance that can occur by adding caps of different diameters to Savonius rotors with different blade structures with approximately the same area and observed that caps with a larger rotor diameter increase the performance significantly. Ali [5] conducted a study experimentally comparing Savonius rotors at low speeds according to the number of blades. In the experimental study, 2- and 3-bladed rotors were produced with certain calculations, their performances were compared under the same test conditions, and it was decided that 2-bladed rotors were more efficient. Altan et al. [6] produced the Savonius wind turbine rotors using 3D printers and then investigated the effect of the change on the performance of the change, which is caused by adding plates of specified dimensions to their blades, both experimentally and numerically. According to the results obtained from the experiments, it was concluded that the compression of the flow in the blades decreased, and the performance of the rotor increased. It was observed that the power coefficient in the rotor increased by 20 percent when the (1/r) ratio was adjusted to 0.3, the (s/r) ratio to 1, and the added plate angle as 135 degrees. Zhao et al. [7] aimed to increase the

\*Corresponding author: youremail@mail.com

power coefficient with the helical Savonius rotors they designed, although the power coefficient of the classical Savonius rotor is about 0.15. In this development, aspect ratio ( $H/D_{Rotor}$ ), overlap ratio, and helix angle were used as variables. As a result of the study, while the aspect ratio was 6, the overlap ratio was 0.3 and the helix angle was 180 degrees, the optimum power coefficient increased to 0.2 (the tip speed ratio was 0.75 at this time). In addition, the starting torque value was better than the conventional rotor. Kharade et al. [8] tried to explain experimentally and theoretically the methods of increasing the overall efficiency of the rotors of vertical axis wind turbines by optimizing them. For Savonius turbines, although not much different from the above-mentioned efficiency-increasing methods, the performance of Savonius rotors with helical blade structures formed by the change of twist angles, according to the number of blades, was examined. As a result of this study, the power coefficient of 2-bladed rotors ( $C_p = 0.53$ ) was found to be greater than that of 3-bladed rotors ( $C_p = 0.36$ ). Zemamou et al. [9] carried out studies to increase the power coefficient of the classical savonius rotor (classic savonius  $C_p$  range varies between 0.1 and 0.25) and because of the geometric improvements they made, they increased the power coefficient to 0.273. Gül and Kolip [10] achieved better results with the split blade designs of the Savonius rotor that they designed, which open and close according to the wind direction, compared to the power coefficient of the classical Savonius rotor ( $C_p = 0.38$ ) and an improvement of 40 percent was observed compared to the other designed models. Jeon et al. [11] investigated the performance change in the wind tunnel by adding caps in different shapes (4 types) to savonius rotors with helical blade structure and changing the diameters of these end plates. In addition, they examined the rotor performance in the without end plate state. According to the results obtained, while the power coefficient values of all of them up to 0.2 are close to each other, after 0.2 it is concluded that the rotor with the end plate is higher in terms of power coefficients than the case without the end plate. In this result, it can easily be seen that it is more than double if the rotor, which is in the full-circle capped state, is compared according to the highest values of the power coefficients compared to its without end plate state.

Although the subjects investigated in this study are separately included in the literature studies, for example, Zhao et. get. [7], the performance changes of the rotors formed by the change of the  $H/D_{Rotor}$  ratios have been examined, and the examination of the produced rotors without end plate condition according to their with end plate condition is given in Akkuş [4] and Jeon [11]. No study was found in which the investigated parameters were compared together. Accordingly, they evaluated the results by comparing their studies according to the data they obtained.

## 2. MATERIALS AND METHODS

### 2.1 Method

All of the produced savonius rotors were created by 3D printers. 3D printers have become frequently used in daily life due to their outstanding performance in various

industries [12]. The produced rotors were investigated experimentally and numerically. Experimentally, it was carried out in the wind tunnel in the Aerodynamics Laboratory of the Faculty of Aeronautics and Astronautics of Erciyes University. As a result of numerical analysis, the experimental setup designed in the cad program was created in the Fluent program. The numerical analysis part was carried out with the data taken from the experimental analysis. More detailed information is given in the numerical analysis section below.

### 2.2 Material

The infill ratio is low so that the rotors are not heavy in terms of aerodynamics. Production was carried out by adhering to the production tolerances of the rotor, depending on the calibration of the printer used. In addition, the end plates are made of medium-density fiberboard material with laser cutting.

Table 1. Printing Parameters of 3D Printed Rotors.

Aspect ratio [ $H/D_{rotor}$ ]	Filament used	Nozzle Temperature [°C]	Table Temperature [°C]	Print Speed [mm/s]	Weights [gr]	Solidity ratio [Infill]	Layer Thickness [mm]	Print Time [Hour]
0.75	esun pla+ [White]	210	20	30	193	10%	0.2	27.35
1	esun pla+ [White]	210	20	30	188	10%	0.2	26.20
1.25	K Camel pla [Black]	210	20	30	198	10%	0.2	25.30
1.5	esun pla+ [White]	210	20	30	189	10%	0.2	25

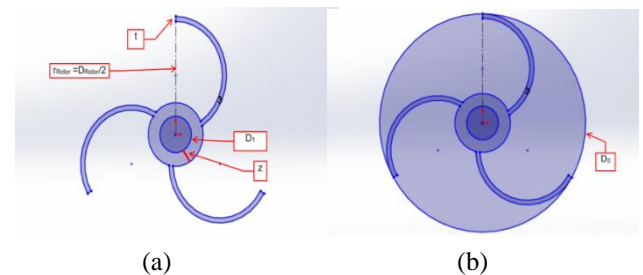


Figure 1. (a) Without endplate and (b) With endplate of the designed rotors (Schematic representation)



Figure 2. Height of designed rotors (Schematic representation)

Table 2. Geometric parameters of 3D printed rotors.

Aspect ratio [H/D Rotor]	Rotor Diameter [D Rotor -mm]	Rotor Cover Diameter [D 0 -mm]	Rotor/Shaft Bore diameter [D 1 -mm]	Rotor Height [H-mm]
0.75	209,761	209,761	10	157,321
1	181,659	181,659	10	181,659
1.25	162,480	162,480	10	203,101
1.5	148,323	148,323	10	222,486

Table 3. Geometric parameters of 3D printed rotors (Continued)

Aspect ratio [H/D Rotor]	Rotor Covers Wall Thickness [mm]	Wing Wall Thickness [t-mm]	Rotor Hole Thickness [z-mm]	Number of Wings
0.75	2.9	5	5	3
1	2.9	5	5	3
1.25	2.9	5	5	3
1.5	2.9	5	5	3

Front view area,

$$A_{front\ view} = H * d_{rotor} \quad (1)$$

where H is the turbine height.

Mechanical power,

$$P_{turbine} = (T * \omega_{turbine}) \quad (2)$$

where T is the torque and  $\omega$  is the Turbine angular velocity.

Wind power,

$$P_{wind} = (\rho A_{front\ view} V_{wind}^3) / 2 \quad (3)$$

where  $\rho$  is the density and  $V_{wind}$  is wind speed.

Tip speed ratio,

$$TSR = (\omega_{turbine} * (d_{rotor}/2) / V_{wind}) \quad (4)$$

Power coefficient,

$$Cp = (P_{turbine}/P_{wind}) \quad (5)$$

The values obtained by analyzing the produced rotors in the experimental environment will be displayed in the graph called TSR/Cp. Above are the theoretical equations related to this subject. The TSR is also known as the tip speed ratio and is the ratio of the linear speed of the turbine to the speed of the wind. Cp is known as the performance or power coefficient and is the ratio of the mechanical power produced by the turbine to the flow power in the wind. The optimum design point is equivalent to the maximum value of the coefficient of performance. produced above the front view area of all the rotors was determined as 330 cm<sup>2</sup> (0.033 m<sup>2</sup>). The main purpose of this study is to examine the performance

changes in the rotors produced by changing the aspect ratios, both with their end plates (the ratio of the end plates of all rotors is determined as  $D_{Rotor} / D_0 = 1$ ) and without the end plate. The fact that all the blades in the produced rotors are straight blades is due to the poor calibration of the 3D printer. Therefore, the resulting Cp values may be lower than those in the literature. In the same way, since the problem of the 3D printer not pulling the filament on time, there were problems in the integrity of the structure, but in general, the structures are suitable for aerodynamic analysis.

### 3. RESULTS

#### 3.1 Experimental Analysis

As mentioned before, the experimental analysis part was carried out in the wind tunnel at the Laboratory of Erciyes University. The dimensions of the tunnel are in meters known as 2.3 m x 1.71 m x 10.6 m, respectively. In addition, the inlet and outlet cross-sections of test section in meters are given as 0.57 m x 0.57 m and 0.59 m x 0.59 m, respectively. This wind tunnel can operate in the range of 3-33 m/s. There is a 15-kW fan in the tunnel. The general view and cad view are given below.



Figure 3. Wind tunnel main view (Erciyes University Faculty of Aeronautics and Astronautics Aerodynamics Laboratory)

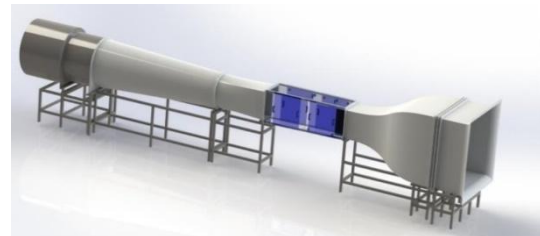


Figure 4. Wind tunnel street view [13]

The laboratory temperature was 15 °C, the density of the air was 1.089 kg/m<sup>3</sup>, and the kinematic viscosity value was  $1.78 \times 10^{-5}$  kg/m·s. The wind speed for the experiments conducted at a constant 10 m/s.

The experimental procedure can be listed as given the rotors were first attached to a carbon-made rod without end plates, and then one end was mounted in the torque meter slot below and the other end was mounted on the

top cover of the tunnel. Then the tunnel was started and waited until the fan reached 10 m/s wind speed. When it reached sufficient speed, the rotors were first intervened manually and then rotated by the wind. Then, the free load of each of them was calculated and the torque (in Nm unit) and angular velocity (in rpm unit) provided by the rotor was read from the torque meter by descending from that load at certain intervals. The rotors that were tested without the end plate were then re-tuned with the end plates attached (the diameter of the caps is equal to the diameter of the rotor). TSR/C<sub>p</sub> graphics were obtained when the values obtained in the table prepared on the computer were entered. The test results for the rotors in the wind tunnel, both with and without the end plate, are shown below.

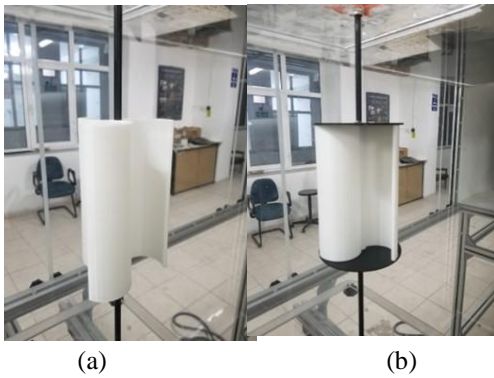


Figure 5. Rotor with 1.5 aspect ratio (a- Without end plate, b- With end plate)

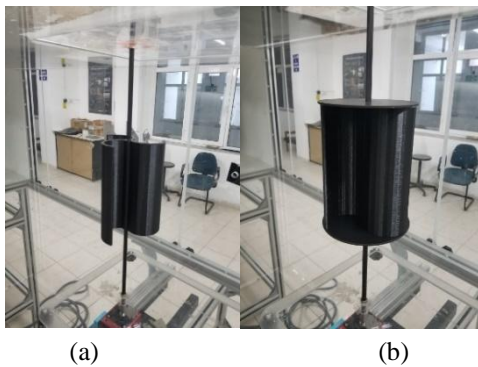


Figure 6. Rotor with 1.25 aspect ratio (a- Without end plate, b- With end plate)

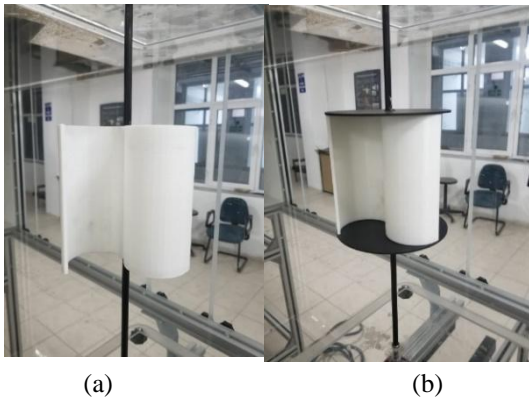


Figure 7. Rotor with 1 aspect ratio (a- Without end plate, b- With end plate)

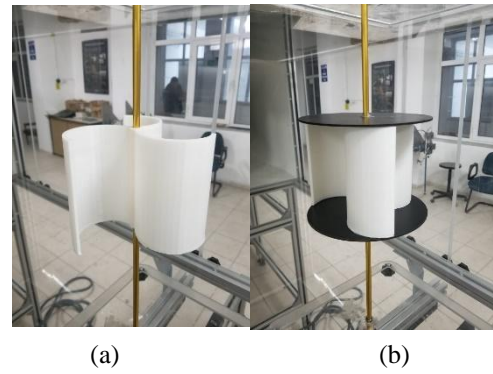


Figure 8. Rotor with 0.25 aspect ratio (a- without end plate, b- With end plate)

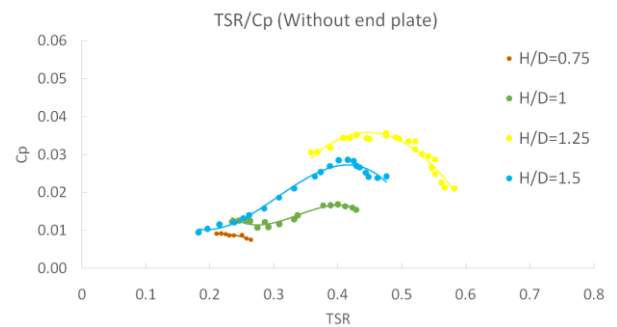


Figure 9. TSR/C<sub>p</sub> graph of rotors (Without end plate)

As can be seen from here, the power coefficients increase significantly as the aspect ratio (H/D) of the rotors increases. In particular, rotors with ratios of 1.25 and 1.5 showed outstanding performance compared to rotors with ratios of 0.75 and 1. Their production challenges and the ensuing weight disparities in performance may also have an impact on how well they perform due to the inferior quality of the filament used to manufacture that rotor compared to the others. In addition, the rotor with a ratio of 1.25 in terms of print quality is better than the others. However, since its compatibility with the 3D printer being printed is better than the others, it is possible to print more smoothly and have better power coefficients accordingly. Another factor affecting their overall performance is that rotors with a ratio of 1.5 and 1.25 have more torque than rotors with a ratio of 0.75 and 1. at the same speed. For example, if the rotors with 1.25, 1.5, and 1 ratio according to their performance are compared for approximately 420 rpm, the rotor with the lowest ratio of 1 followed by 1.5 and the rotor with the highest torque value was 1.25. In addition, the high torque also affected the pressure values that the rotors met due to air at the same rate. This can be given to the relationship between the magnitude of the thrust in the torque equation and the radius of the rotors. In addition, the increase in this pressure caused an increase in the power coefficient. This can be seen in the pressure graphs in the numerical analysis below.

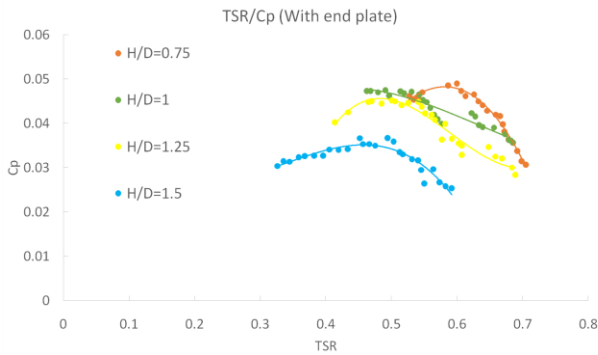


Figure 10. Variation of  $TSR/C_p$  (With end plate)

At this time, as the aspect ratio of the rotors becomes smaller, the difference between the power coefficients was small compared to bare case, but it still increased the power coefficients. Here, rotors with a ratio of 0.75 to 1 performed exceptionally well compared to rotors with a ratio of 1.25 to 1.5. Although all rotors have increased their performance compared to their uncapped condition, especially the rotors with the ratios of 1.5 and 1.25 could not increase as much as the rotors with the ratios of 0.75 and 1. The feature that increases the torque in their general performance is the increase in torque and the increase in pressure due to the addition of the effect of the cap on the rotors to the relationship between the thrust force and the radius. A point that should be noted here is that when their performance is compared to their uncapped situation, a torque increase of almost 3 times has been observed for their graphics, especially in the rotors with the ratios of 1 and 0.75, both in the without end plate and with end plate conditions at similar revolutions.

### 3.2 Numerical Analysis

Numerical analysis was carried out in the ANSYS FLUENT program, as mentioned before. The relevant models were modeled in an external CAD program and transferred to the Ansys program and then to the Fluent part. Since the deviation in the dimensions of the wind tunnel will disrupt the mesh layout, the average of both the entrance and the exit of the tunnel is modeled as 0.58 m x 0.58 m in meters. The total length of the tunnel is 2.7 meters, and the modeled area (rod) is positioned at a distance of 0.9 meters from the entrance part so that the rotors can rotate. In addition, the dimensions of the part called the rod are a cylinder with a radius of 0.15 meters and a height of 0.3 meters, and it is modeled in such a way that it can be placed easily in all rods. The initial layout of the rotor blades is shown below, with the rotor with an aspect ratio of 1.5 as an example model, without end plate. In addition, the hole part, which is suitable for connecting the rotors with a rod as in the experimental analysis, was filled with the extrusion command while creating the cad model of the rotors. Otherwise, it affects the analysis result, and it is modeled in this way since it is seen as if the fluid is passing through the hole in the display of the flow profiles.

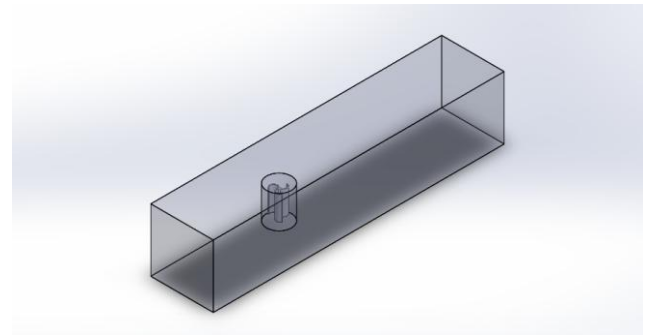


Figure 11. Representation of the model to be used in the analysis (Rotor with 1.5 aspect ratio)

If the analysis will be made here and which parameters will be taken as a basis in such analyzes, the first two rotors with the best  $TSR/C_p$  points -the aspect ratios of 1.5 and 1.25 for the ones without end plate, the rotors with the aspect ratio of 0.75 and 1 for the end plates- steady were analyzed. In addition, additional steady analyzes were created for flow monitoring purposes to examine the performance of the rotors at the same angular velocities in terms of comparing each other (with and without end plate in their groups) according to the differences in the experimental results. It is determined that these rotors are 588 rpm in their capped condition and 420 rpm in their uncapped condition. However, the point to be noted here is that the rotor, which has a 0.75 ratio in uncapped situations, performs worse than the others, so it will not be displayed in a capless state. The velocity and pressure contour images taken in each of these analyzes are given below. It is not possible to carry out the analysis within the scope of the assignment, as the validation processes will be quite long. In addition, this method was used because the validations should have reached the appropriate mesh structure and mesh independence, and the results should be as close to the data obtained from the experiments as possible.

Required meshstructures, name definitions, and required values are shown in the meshtable below. Since the reduction of meshes increases both the time and the overall number in the analysis, the smallest possible meshes were discarded and corrected in the polyhedral mesh part in a fluent environment. Also meshes Ansys fluent It was made following the quality values found in the [14] guideline, and the quality values were created close to the limits in this guide.

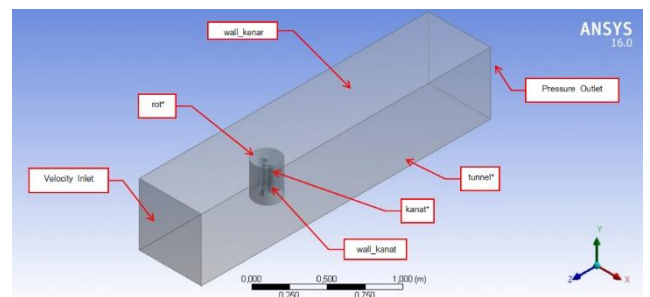


Figure 12. Naming the model to be used in the analysis (Rotor with 1.5 aspect ratio)

The nomenclature with an asterisk on them represents the geometric names, and the rest represent the nomenclature to be used in the analysis. Interface definitions are named between the rod and tunnel surfaces. It has been said before that after the required mesh quality values are provided, pressure-based steady analyzes are made in the Ansys /Fluent program. Since there will be airflow inside the modeled tunnel, the gravitational acceleration is not that effective. Therefore, the gravitational acceleration part remained closed. The input values of the analyzes to be performed at a steady state were taken from the experimental data.

SST k- $\omega$  model, which can solve aerodynamic analyzes better than other models based on recent academic studies [15]. When the necessary data were entered on the rod (available in the mesh table), the element that will rotate as intended, the entrance and sections of the tunnel, the analyzes were started and according to the result, both the velocity and pressure contours of the analyzes were taken and transferred here.

Table 4. Mesh parameters of rotors prepared for numerical analysis (All mesh commands not mentioned here are left in standard settings in the program).

Mesh Table			
Aspect ratio (H/ D <sub>rotor</sub> )	General Mesh Method	Local Mesh Method	Inflation (Boundary Layer) Method
0.75 - Without End Plane	Relevance-100/ Relevance Center-Fine / Smoothing -High	Sizing ( rot - all body) - 5mm	smooth Transition - 20 Layers
0.75 - With End Plane	Relevance-100/ Relevance Center-Fine / Smoothing -High	Sizing ( rot - all body) - 3mm	smooth Transition - 20 Layers
1 - Without End Plane	Relevance-100/ Relevance Center-Fine / Smoothing -High	Sizing ( rot - all body) - 5mm	smooth Transition - 20 Layers
1 - With End Plane	Relevance-100/ Relevance Center-Fine / Smoothing -High	Sizing ( rot - all body) - 3mm	smooth Transition - 20 Layers
1.25 - Without End Plane	Relevance-100/ Relevance Center-Fine / Smoothing -High	Sizing ( rot - all body) - 5mm	smooth Transition - 20 Layers
1.25 - With End Plane	Relevance-100/ Relevance Center-Fine / Smoothing -High	Sizing ( rot - all body) - 3mm	smooth Transition - 20 Layers
1.5 - Without End Plane	Relevance-100/ Relevance Center-Fine / Smoothing -High	Sizing ( rot - all body) - 5mm	smooth Transition - 20 Layers
1.5 - With End Plane	Relevance-100/ Relevance Center-Fine / Smoothing -High	Sizing ( rot - all body) - 3mm	smooth Transition - 20 Layers

Table 5. Mesh quality values of rotors (Ansys according to fluent guide) – Without end plane.

Quality Values						
Element Quality						
Aspect Ratio (H/ D <sub>rotor</sub> )	Minimum	Maximum Value	Average Value	Deflection	Node	Element
0.75	0.0013508	1	0.6152	0.35357	400601	1416339
1	0.0030653	1	0.63781	0.34275	450761	1647751
1.25	0.0028844	1	0.63428	0.34441	462741	1681616
1.5	0.0029779	1	0.63054	0.34577	475660	1718988
Orthogonal Quality						
Aspect ratio (H/ D <sub>rotor</sub> )	Minimum	Maximum Value	Average Value	Deflection	Node	Element
0.75	0.010355	0.99973	0.85181	0.14358	400601	1416339
1	0.019847	0.99956	0.85458	0.13205	450761	1647751
1.25	0.020251	0.99958	0.85402	0.113199	462741	1681616
1.5	0.019359	0.99941	0.85333	0.13174	475660	1718988
Skewness						
Aspect Ratio (H/ D <sub>rotor</sub> )	Minimum	Maximum Value	Average Value	Deflection	Node	Element
0.75	3.9961E-08	0.8496	0.22464	0.13629	400601	1416339
1	2.6512E-09	0.83892	0.22514	0.13286	450761	1647751
1.25	5.88E-08	0.84225	0.22599	0.13159	462741	1681616
1.5	1.9015E-08	0.84561	0.22674	0.13118	475660	1718988

Table 6. Mesh quality values of rotors (Ansys according to the fluent guide) - With end plane.

Quality Values						
Element Quality						
Aspect Ratio (H/ D <sub>rotor</sub> )	Minimum	Maximum Value	Average Value	Deflection	Node	Element
0.75	0.00056418	1	0.64077	0.34183	1416700	5227374
1	0.0013066	1	0.65871	0.33334	1350220	5142735
1.25	0.0014164	1	0.67105	0.34441	1306853	5086620
1.5	0.00070041	1	0.67731	0.32353	1289496	5080500
Orthogonal Quality						
Aspect Ratio (H/ D <sub>rotor</sub> )	Minimum	Maximum Value	Average Value	Deflection	Node	Element
0.75	0.014166	0.9999	0.87239	0.12019	1416700	5227374
1	0.01449	0.99992	0.87121	0.11812	1350220	5142735
1.25	0.016188	0.99992	0.87024	0.11764	1306853	5086620
1.5	0.014206	0.99975	0.86907	0.11738	1289496	5080500
Skewness						
Aspect Ratio (H/ D <sub>rotor</sub> )	Minimum	Maximum Value	Average Value	Deflection	Node	Element
0.75	2.0853E-09	one	0.20899	0.13154	1416700	5227374
1	2.0851E-09	0.93733	0.20865	0.13017	1350220	5142735
1.25	2.1347E-09	0.93003	0.20886	0.12915	1306853	5086620
1.5	2.1311E-09	0.92284	0.21037	0.12849	1289496	5080500

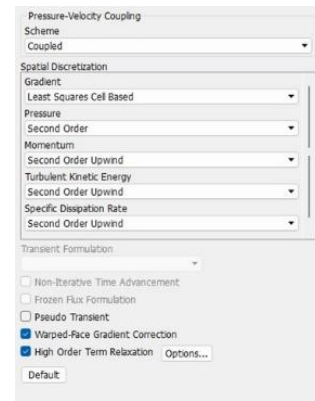


Figure 13. Solution method and parameters to be used in analysis

In the analysis program, the solution methods were applied as shown in the above figure in all of the analyzes performed as steady on the flow images. In the analyzes performed in steady-state, the analysis was completed with 2000 iterations.

As mentioned before, the inconsistency of numerical analyzes with experimental analyzes is not due to the input values written in the program, but to the appropriate mesh number and the inability to reach a solution independent of this mesh number. The data obtained from the numerical analyzes were used only to compare the data obtained from the experimental analyzes with each other.

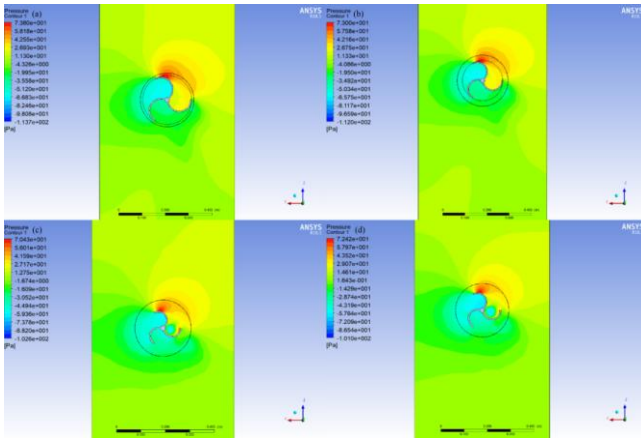


Figure 14. Pressure distribution on XZ plane of rotors with aspect ratio of a-0.75 (With end plane and  $n = 546$  rpm), b-1 (With end plane and  $n = 516$  rpm), c-1.5 (Without end plate and  $n = 534$  rpm) and d-1.25 (Without end plate and  $n = 558$  rpm)

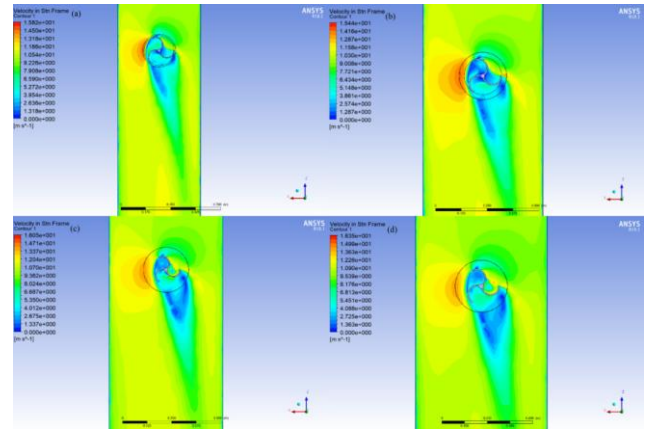


Figure 16. Velocity distribution on the XZ plane of rotors with aspect ratio of a-0.75 (With end plane and  $n = 546$  rpm), b-1 (With End Plane and  $n = 516$  rpm), c-1.5 (Without end plate and  $n = 534$  rpm) and d-1.25 (Without end plate and  $n = 558$  rpm)

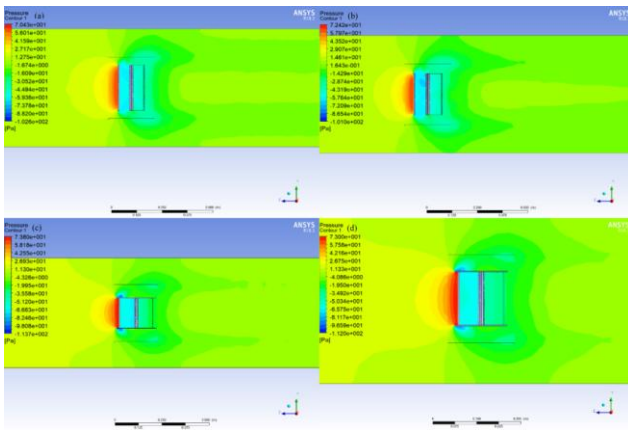


Figure 15. Pressure distribution on the YZ plane of rotors with aspect ratio of a-0.75 (With end plane and  $n = 546$  rpm), b-1 (With End Plane and  $n = 516$  rpm), c-1.5 (Without end plate and  $n = 534$  rpm) and d-1.25 (Without end plate and  $n = 558$  rpm)

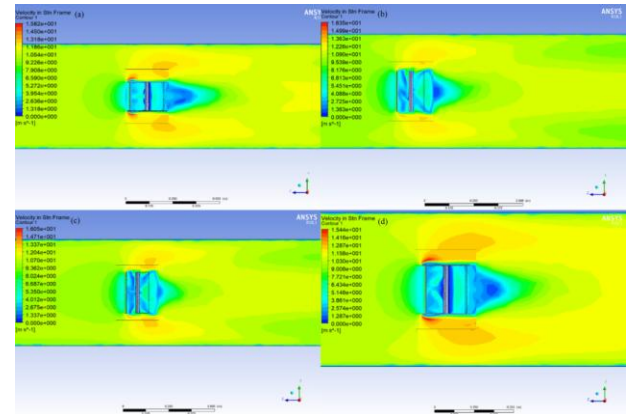


Figure 17. Speed distribution on the YZ Plane of rotors with aspect ratio of a-0.75 (With end plane and  $n = 546$  rpm), b-1 (With End Plane and  $n = 516$  rpm), c-1.5 (Without end plate and  $n = 534$  rpm) and d-1.25 (Without end plate and  $n = 558$  rpm)

The representations in the XZ and YZ planes in figures 14 and 15, with the angular velocity values corresponding to the values in the maximum power coefficient obtained from the experimental analysis of the rotors with aspect ratio 0.75 (without end plate), 1 (without end plate), 1.25 (with end plate) and 1.5 (with end plate). The pressure distribution obtained from the numerical analyzes made is observed. As observed, negative pressure was observed in the rotors without end plate. However, this was not observed in rotors with end plates. This is also observed in the case of the rotors with and without the end plate, which have the same aspect ratio. In other words, in the case of uncapped rotors with end plates, this negative pressure disappears and it is observed that the torque values increase when compared with the ensuing torque increase at the same angular speeds. This is basically what is meant here.

The representations in the XZ and YZ planes in figures 16 and 17, with the angular velocity values corresponding to the values in the maximum power coefficient obtained from the experimental analysis of the rotors with aspect ratio 1.25 (without end plate), 1.5 (without end plate), 1 (with end plate) and 0.75 (with end plate). The velocity distribution obtained from the numerical analyzes made is observed. As observed, speed drops due to negative pressure were observed in rotors without end plate. However, this was not observed in rotors with end plates. This is also observed in the case of the rotors with and without the end plate, which have the same aspect ratio. In other words, when the rotors without end plate are end plates, this negative pressure disappears and it is observed that the torque values increase when compared with the subsequent torque increase at the same angular speeds. It can be said that a stable flow opportunity is also offered

Table 7. Torque values from analyzes

Name	Experimental		Numerical		Relative Error (%)
	n (rpm)	T (Nm)	n (rpm)	T (Nm)	
With End Plate -0.75-Rotor	546	0.0154	546	0.0249	61,6883
With End Plate -1-Rotor	516	0.0158	516	0.0208	31,6456
Without End Plate -1.25-Rotor	558	0.011	558	0.0164	49,0909
Without End Plate -1.5-Rotor	534	0.0092	534	0.0104	13.0435

Table 7 above shows the rotational numbers of the first two rotors with the maximum power coefficients according to the results of the experimental analyzes of the rotors (with/without end plate) and the experimental and numerical values of the torque values according to these revolutions. In addition, the pressure and velocity indications of the analyzes made for flow monitoring against these numerical values are shown above. Although the numerical data in Table 7 do not agree with the experimental data, the images made support the inferences made from the experimental analysis. In addition to this, additional numerical analyzes (steady) were made to compare the rotors with and without the end plate themselves. In addition to displaying the pressure and velocity distributions from these analyzes, vectorial velocity distributions were taken to examine how the air behaves during the movement of the rotors. In Table 7, in order to reduce the difference between the torque values obtained from numerical analyzes and experimental analyzes, even though it is tried to approach realistic results by entering the roughness values in the wall definition in the rotor part in the numerical analysis, there is not much difference in the results obtained.

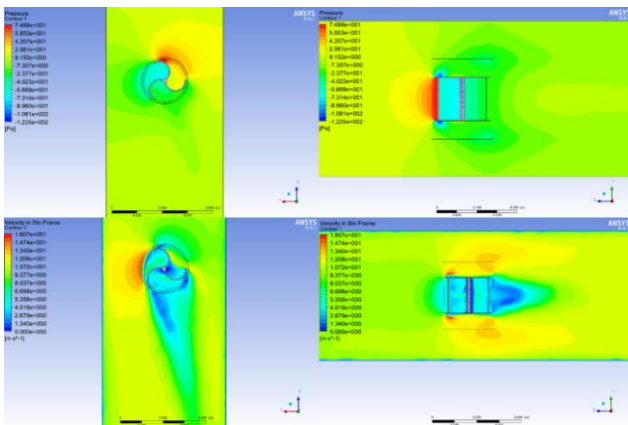


Figure 18. Pressure and velocity distribution on XZ and YZ planes of a rotor with aspect ratio of 0.75 (With end plate) (n = 588 rpm)

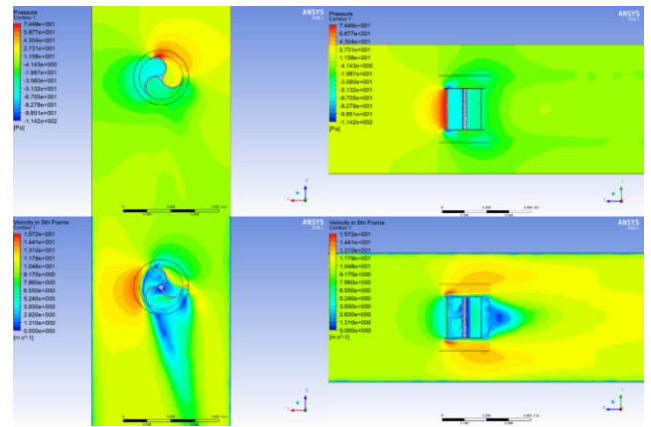


Figure 19. Pressure and velocity distribution on XZ and YZ planes of a rotor with aspect ratio of 1 (With end plate) (n = 588 rpm)

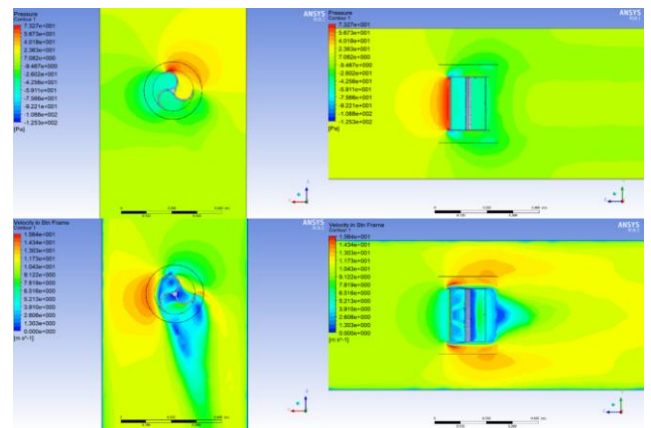


Figure 20. Pressure and velocity distribution on XZ and YZ planes of a rotor with aspect ratio of 1.25 (With end plate) (n = 588 rpm)

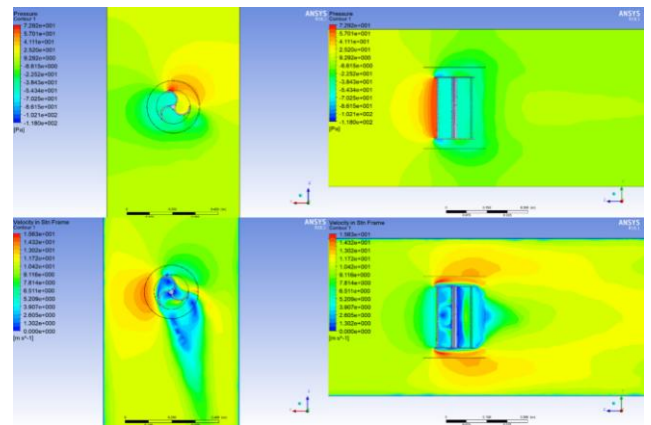


Figure 21. Pressure and velocity distribution on XZ and YZ planes of a rotor with aspect ratio of 1.5 (With end plate) (n = 588 rpm)

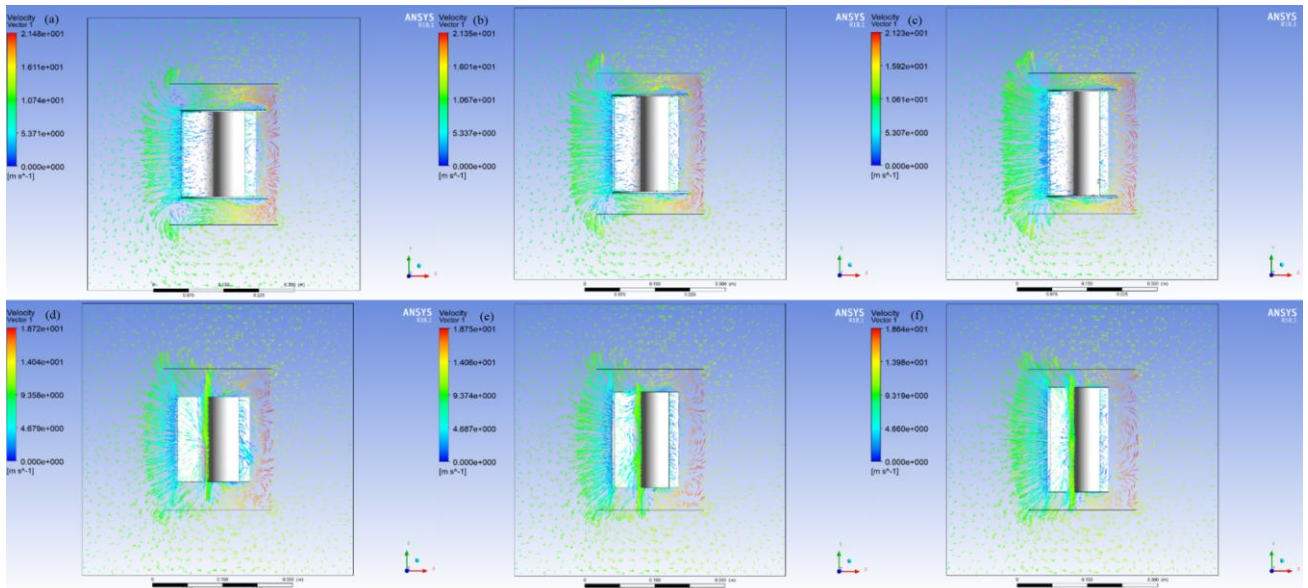


Figure 22. Vectorial velocity distribution on XY plane of rotors with aspect ratio of a-1 (With end plate and  $n = 588$  rpm), b- 1.25 (With end plate and  $n = 588$  rpm), c- 1.5 (With end plate and  $n = 588$  rpm), d- 1 (Without end plate and  $n = 420$  rpm), e-1.25 (Without end plate and  $n = 420$  rpm) and f- 1.5 (Without end plate and  $n = 420$  rpm).

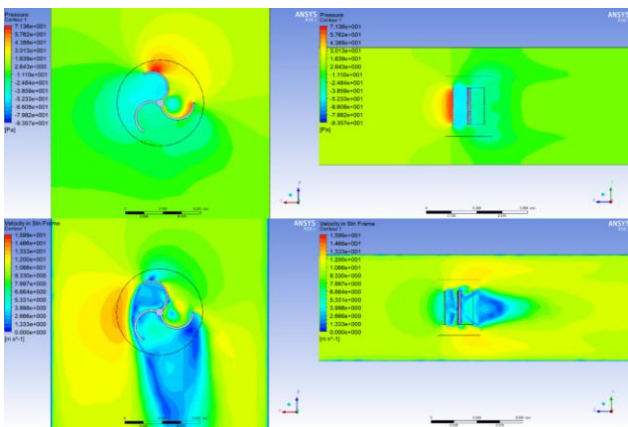


Figure 23. Pressure and velocity distribution on XZ and YZ planes of a rotor with aspect ratio of 1 (Without end plate) ( $n = 420$  rpm)

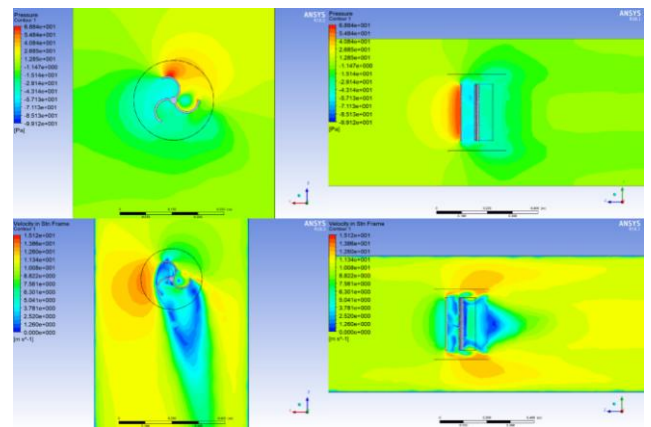


Figure 25. Pressure and velocity distribution on XZ and YZ planes of a rotor with aspect ratio of 1.5 (Without end plate) ( $n = 420$  rpm)

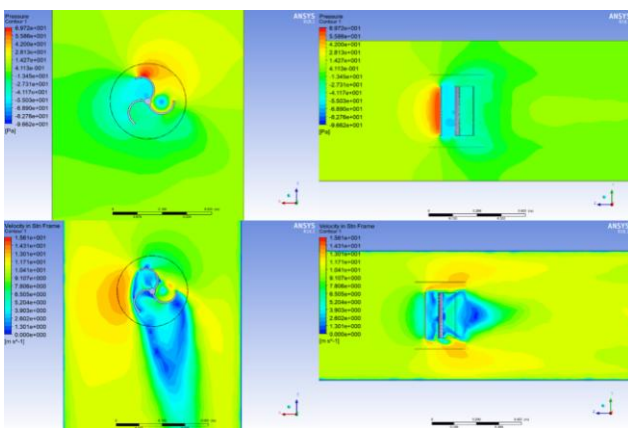


Figure 24. Pressure and velocity distribution on XZ and YZ planes of a rotor with aspect ratio of 1.25 (Without end plate) ( $n = 420$  rpm)

## 4. DISCUSSION AND CONCLUSION

### 4.1 Discussion

The pressure-velocity distributions of capped rotors at 588rpm (fig. 18-21) and the pressure-velocity distribution of uncapped rotors at 420rpm (fig. 23-25) are shown above. While the aspect ratios of 0.75, 1, 1.25, and 1.5 were examined respectively in capped cases, rotors with 1, 1.25, and 1.5 ratios were examined in caseless ones, respectively. The rotor with end plates aspect ratio of 0.75 was not included in the comparison since the desired rpm speeds were not achieved experimentally. Looking at the inside of the blade that meets the air of the covered rotors, it is smooth and the maximum pressure value of 0.75 is read, respectively, and the smallest pressure value is seen at 1.5 (Figures 18-21). Although the values shown in the pressure distribution seem close to each other, they differ in terms of the penetration of the pressures and support the experimental studies. Negative pressure was observed

inside the blade that meets the air in the flow imaging of the rotors without end plate (Figures 23-25). The reason for this is that the air cannot be trapped inside the blade in rotors without end plate. In addition, the pressure drops due to the eddy flow in the blade and around the rotor caused a decrease in the torque and power coefficient. The vectorial movements of the pair shown in Figures 22, also support this situation. In the experimental study, it has been observed that 1.25 has higher efficiency than 1.5 in the rotors without end plate. The reason for this is that in the numerical study, higher negative pressure was observed in the rotor blade with a ratio of 1.5, seen in figures 23 and 24, compared to 1.25.

In general, when the rotors are compared with and without the end plate, according to the results obtained from the experimental analysis, it has been observed that the torque (power) produced in the closed cases at the same rpm values is higher than the torque produced without the end plate. Due to the numerical imaging made earlier, the efficiency decrease due to the negative pressure in the capless ones was not observed in the capped state, and it caused an abnormal increase in efficiency in some rotors (example 0.75).

#### 4.2 Conclusion and Suggestions

According to the results obtained from the analysis, rotors with small aspect ratios in the case of the rotors without end plate have lower power coefficients and their overall performances have increased with the increase in aspect ratios. It has been concluded that the pressure values encountered by the rotors are directly related to the power coefficients they produce. However, the opposite effect was observed this time in the analysis of the rotors with the end plate. Here, the low aspect ratios caused the power coefficients to increase more than the others. The numerical analyzes performed for flow monitoring to compare the rotors with each other in both without the end plate and with the end plate states at equal revolutions also agree with the results obtained from the experimental analyzes.

#### Acknowledgments

Who provided to us with all kinds of help and sacrifices during our work, we would like to thank my esteemed teachers Prof. Dr. Selahaddin Orhan AKANSU and Prof. Dr. Sebahattin ÜNALAN.

#### REFERENCES

[1] S. R. Paramatia, U. Shahzad and B. Doğan, The role of environmental technology for energy demand and energy efficiency: Evidence from OECD countries, *Renewable*

and Sustainable Energy Reviews, vol. 153, pp. 111735, 2022.

[2] O. Edenhofer, et al., *Renewable energy sources and climate change mitigation: Special report of the intergovernmental panel on climate change*, Cambridge University Press, 2011.

[3] B. Metz, O. R. Davidson, P. R. Bosch, R. Dave, and L. A. Meyer, *IPCC Climate Change 2007: Mitigation of Climate Change*, Cambridge University Press, 2007.

[4] M. B. Akkuş, Z. Haksever and S. Teksin, *Experimental and Numerical Analysis of Savonius Wind Turbine with End Plate on Various Types*, *Energy, Environment and Storage*, vol. 2, pp. 61-70, 2022.

[5] M. H. Ali, *Experimental comparison study for Savonius wind turbine of two & three blades at low wind speed*, *International Journal of Modern Engineering Research*, vol. 3, pp. 2978-2986, 2013.

[6] B. D. Altan, G. Altan and V. Kovan, *Investigation of 3D printed Savonius rotor performance*, *Renewable Energy*, vol. 99, pp. 584-591, 2016.

[7] Z. Zhao, et al., "Research on the improvement of the performance of Savonius rotor based on numerical study," *2009 International Conference on Sustainable Power Generation and Supply*, IEEE, 2009.

[8] V. Kharade and K. Jagtap, *A Review Study on Vertical axis Wind Turbines (lift and drag type) for Optimizing the Aerodynamic and Structural Performance*, *IOSR Journal of Engineering*, vol. 3, pp. 61-65, 2019.

[9] M. Zemamou, M. Aggour and A. Toumi, *Review of savonius wind turbine design and performance*, *Energy Procedia*, vol. 141, pp. 383-288, 2017.

[10] İ. Gül and A. Kolip, *Parça Kanatlı Savonius Rüzgâr Türbin Performansının İncelenmesi*, *El-Cezerî Journal of Science and Engineering*, vol. 5, pp. 816-827, 2018.

[11] K. S. Jeon, J. I. Jeong, J. K. Pan, and K. W. Ryu, *Effects of end plates with various shapes and sizes on helical Savonius wind turbines*. *Renewable energy*, vol. 79, pp. 167-176, 2015.

[12] C. Schubert, M. C. Van Langeveld and L. A. Donoso, *Innovations in 3D printing: a 3D overview from optics to organs*, *British Journal of Ophthalmology*, vol. 98, pp. 159-161, 2014.

[13] İ. Yılmaz, Ö. Çam, M. Taştan and A. Karcı, *Experimental Investigation of Aerodynamic Performance of Different Wind Turbine Airfoils*, *Journal of Polytechnic*, vol. 19, pp. 577-584, 2016.

[14] ANSYS Fluent Theory Guide 15.0, ANSYS, 2013.

[15] M. A.A. Nawar, et al. *On the enhancement of Savonius Bach-type rotor performance by studying the optimum stator configuration*, *Ocean Engineering*, vol. 217, pp. 107954, 2020.